Physica B: Condensed Matter 552 (2019) 62–70

Contents lists available at ScienceDirect

Physica B: Condensed Matter

journal homepage: www.elsevier.com/locate/physb

Kramers–Kronig calculations for linear and nonlinear optics of nanostructured methyl violet (CI-42535): New trend in laser power attenuation using dyes

Mohammed A. Assiri[a], M. Aslam Manthrammel[b], A.M. Aboraia[c,d,*], I.S. Yahia[b,e], H.Y. Zahran[b,e], V. Ganesh[b], Mohd Shkir[b], S. AlFaify[b], Alexander V. Soldatov[c]

[a] Advanced Materials and Green Chemistry Lab., Chemistry Department, Faculty of Science, King Khalid University, P.O. Box 9004, Abha, Saudi Arabia
[b] Advanced Functional Materials & Optoelectronic Laboratory (AFMOL), Department of Physics, Faculty of Science, King Khalid University, P.O. Box 9004, Abha, Saudi Arabia
[c] The Smart Materials Research Centre, Southern Federal University, 5 Zorge Street, Rostov-on-Don, 344090, Russia
[d] Department of Physics, Faculty of Science, Al-Azhar University, Assiut, 71542, Egypt
[e] Nanoscience Laboratory for Environmental and Bio-Medical Applications (NLEBA), Semiconductor Lab., Metallurgical Lab. 2 Physics Department, Faculty of Education, Ain Shams University, Roxy, 11757, Cairo, Egypt

ARTICLE INFO

Keywords:
Kramers–Kronig calculations
Methyl violet-10B thin films
Linear/non-linear optics
Dielectric constant and laser power attenuation

ABSTRACT

In this work, nanostructured methyl violet-10B (MV-10B) thin films of various thicknesses were coated on glass substrates by a low-cost spin coating method at different rpm. The structural analysis of nanostructured MV-10B thin films was carried out by X-ray diffraction and atomic force microscope. Optical measurements were carried out, and the direct band gap of MV-10B films was estimated. The study showed that the prepared MV-10B thin films act in the same manner as that of conventional direct bandgap semiconductors. From optical studies, the sample exhibited bandpass filter characteristics in IR range from 700 nm to 900 nm and in the visible range centered around 408 nm. Also, the sample absorbs or attenuates the range of wavelengths in the visible spectrum between 470 and 650 nm creating a good absorption band valley making a CUT-OFF laser filter. Optical constants such as refractive index (n) and extinction coefficient (k) were computed using Kramers–Kronig relations. The real and imaginary components of dielectric constant were calculated on the basis of polarization of light when it is impinging on semiconductors. Nonlinear index of refraction and susceptibilities were estimated by linear refractive index dispersion principles. Optical limiting studies showed that the MV-10B thin films are very good optical limiters even at low thickness. The MV-10B showed a laser attenuation behavior for He-Ne and green lasers. The obtained results suggest that the newly designed thin films are the promising candidate in different applications.

1. Introduction

The booming of nanostructured semiconductors has empowered rapid scientific advances for various opportunities in numerous device fabrications [1]. Compared to bulk counterparts, nanostructured semiconductors with various morphologies have found enormous applications due to their superior technological improvements [2]. Nanostructured organic semiconductors have huge environmental effects on green energy technologies such as solar cells and fuel cells and other optoelectronic devices. Thin films of organic semiconductors have attracted the researchers in near past due to their distinctive optical, electronic and photoelectric properties in comparison with typical inorganic semiconductor based thin films. They have also the advantage of low cost and easy fabrication in large scale by simple methods in addition to their diverse applications in electronics and optoelectronics [3–5]. The organic dyes are also natural nominees of π-conjugated organic materials for efficient light harvesting in dye-sensitized solar cells [6–9].

Methyl violets (MVs) are aromatic organic dyes comprised of hexamethyl, pentamethyl or tetramethyl pararosanilines belonging to the triphenylmethane group. MV dyes are classified into different types based on the methyl quantity linked to the amine functional group [10]. The tetramethyl having four methyl group is termed as MV-2B while pentamethyl and hexamethyl are termed as MV-6B and MV-10B,

* Corresponding author. The Smart Materials Research Centre, Southern Federal University, 5 Zorge Street, Rostov-on-Don, 344090, Russia. Tel.: +7 9526093539.
E-mail addresses: a.m.aboraia@gmail.com (A.M. Aboraia), dr_isyahia@yahoo.com, isyahia@gmail.com (I.S. Yahia), dr_hyzahran@yahoo.com (H.Y. Zahran).

https://doi.org/10.1016/j.physb.2018.09.040
Received 6 August 2018; Received in revised form 20 September 2018; Accepted 27 September 2018
Available online 29 September 2018
0921-4526/ © 2018 Elsevier B.V. All rights reserved.

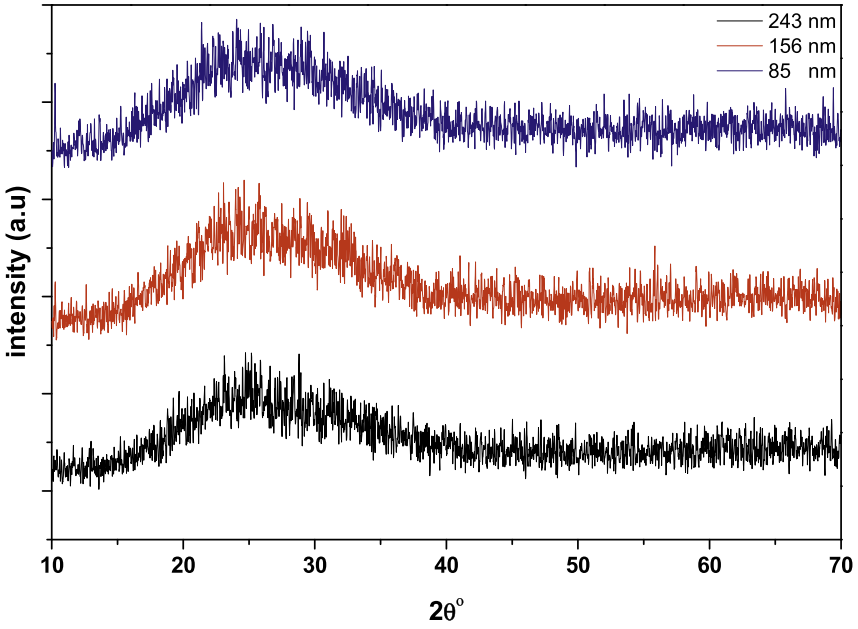

Fig. 1. XRD diffraction patterns of MV-10B thin films of different thicknesses.

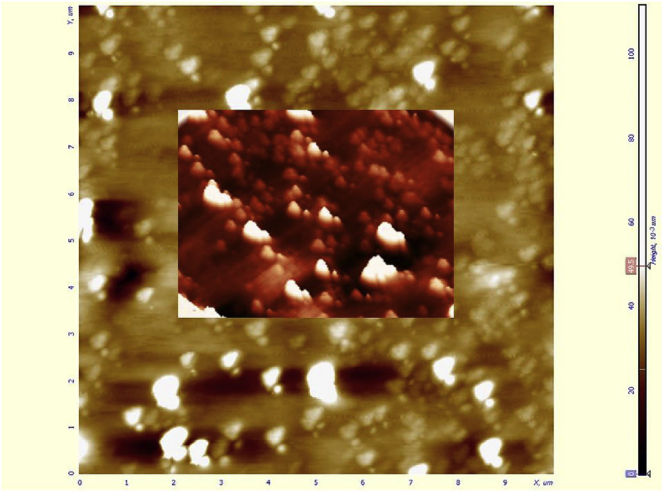

Fig. 2. 2D/3D-AFM analysis of MV-10B thin films of thickness 156 nm (as a representative example).

respectively. Among all MV dyes, MV-2B is the most studied dye as colorant, a biological stain, and semiconductor in addition to its various applications in photodegradation studies and biological treatments [11–14]. Methyl violet-10B (MV-10B) (also known as Hexamethyl pararosaniline chloride, Gentian violet, and crystal violet) is having a molecular formula $C_{25}H_{30}N_3Cl$ and found its potential use in anti-mitotic and antifungal applications. Not much work has been reported on the thin films of MV-10B and hence the spectral response analysis and optical constant details about the MV-10B have yet to be explored. Various procedures have been adopted for the synthesis of dye-based thin films which include spin coating, thermal evaporation, spray pyrolysis and chemical vapor deposition …. etc. [15].

In the present work, up to our knowledge, there is no any reported data about the MV-10B and their application in the field of organic semiconductors. Thin films of MV-10B of various thicknesses were deposited on the glass with the help of spin coater. In present work, Kramers-Kronig dispersion relations are used to calculate the optical constants of all MV-10B thin films by UV–Vis diffused reflectance data [16,17]. Refractive and absorption index and their related parameters were deduced and analyzed.

2. Experimental information

2.1. Thin films deposition

Methyl violet (MV-10B) dye with color index (CI-42535) was procured from Sigma-Aldrich Pvt. Ltd. and was used without any further purification. 10^{-2} M of MV-10B solution was prepared in 20 ml of high purity ethanol and mixed through magnetic stirring at room temperature. After achieving the homogeneous solution its filtration was done and housed in dark place. The previous methodology was applied to clean the substrate [18]. MV-10B thin films with various thicknesses were coated on glass substrates by changing the rotation speed of the spin coater at 1500, 2500 and 3000 rpm.

2.2. Devices and measurements

X-ray diffraction (XRD) data were recorded for all films using a Shimadzu XRD-6000 in an angular range from 10° to 70° [18].

Surface morphology of MV-10B thin films was analyzed through atomic force microscope (AFM) (NT-MDT, Next (Russia)) and size of grains and roughness were analyzed by special software attached to AFM device.

Absorbance *abs(λ)*, transmittance *T(λ)* and reflectance *R(λ)* of all films as a function of wavelength were recorded using UV–Vis–NIR, JASCO V-570 spectrophotometer in 270–1000 nm wavelength range at 300 K.

The optical limiting measurements were measured by using the Z-scan system. A He–Ne laser having wavelength 632.8 nm with input power = 343.1 μW and a solid-state green laser operated at 532 nm with input power 13.62 mW was used. The samples were mounted on the focal length of a lens which was placed on the laser beam path to focus the laser on the sample. An optical power meter fixed at 632 nm was used to measure the laser beam power with and without the sample.

Thin film thicknesses of MV-10B onto glass were estimated by Alpha-Step IQ-device and average values of methyl violet thin films' thicknesses were calculated as follows: 243, 156 and 85 nm corresponding to 1500, 2500 and 3000 rpm of the spin coater, respectively.

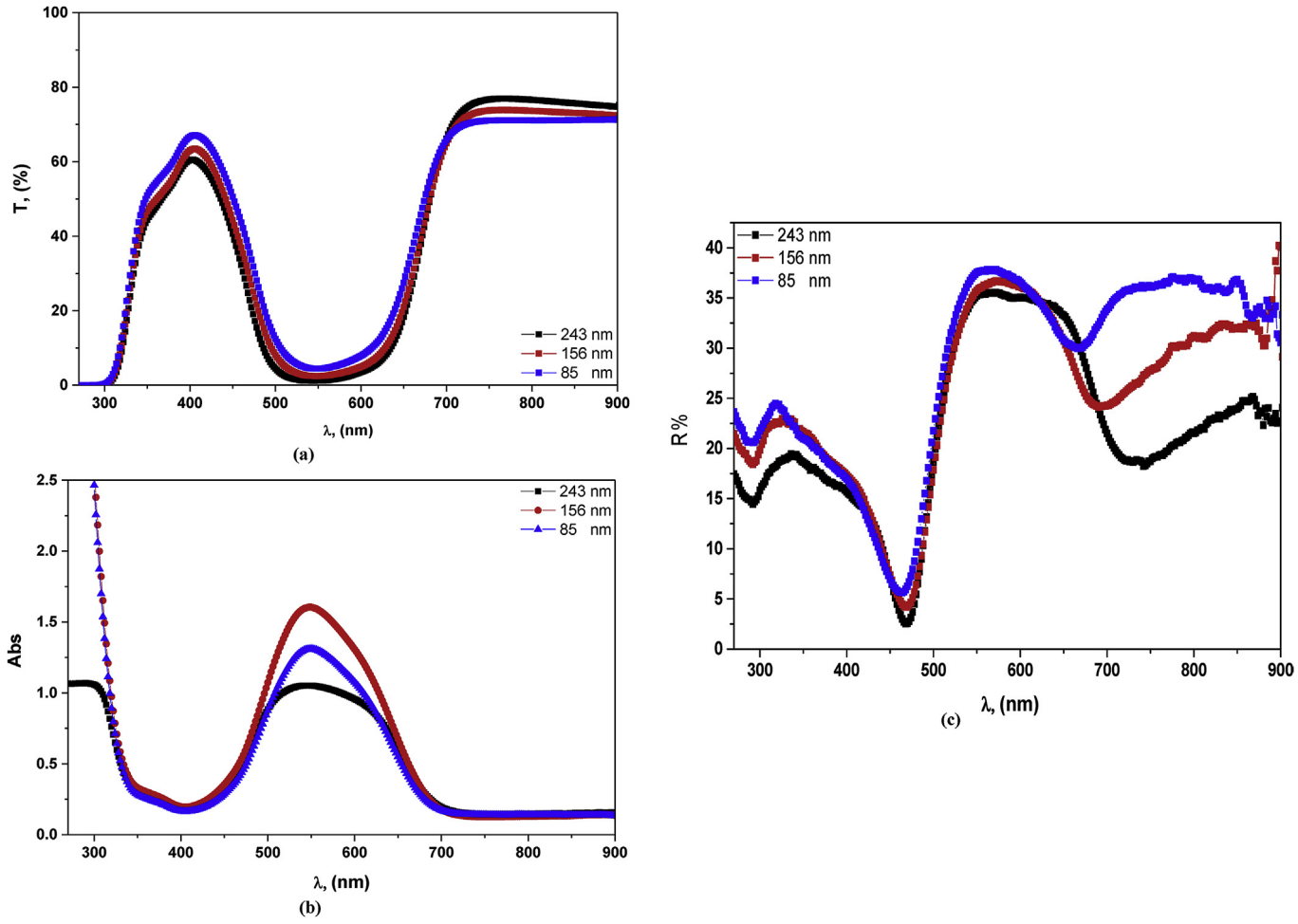

Fig. 3. (a) Transmission, (b) Absorbance and (c) Reflectance spectra of MV-10B thin films of different thicknesses.

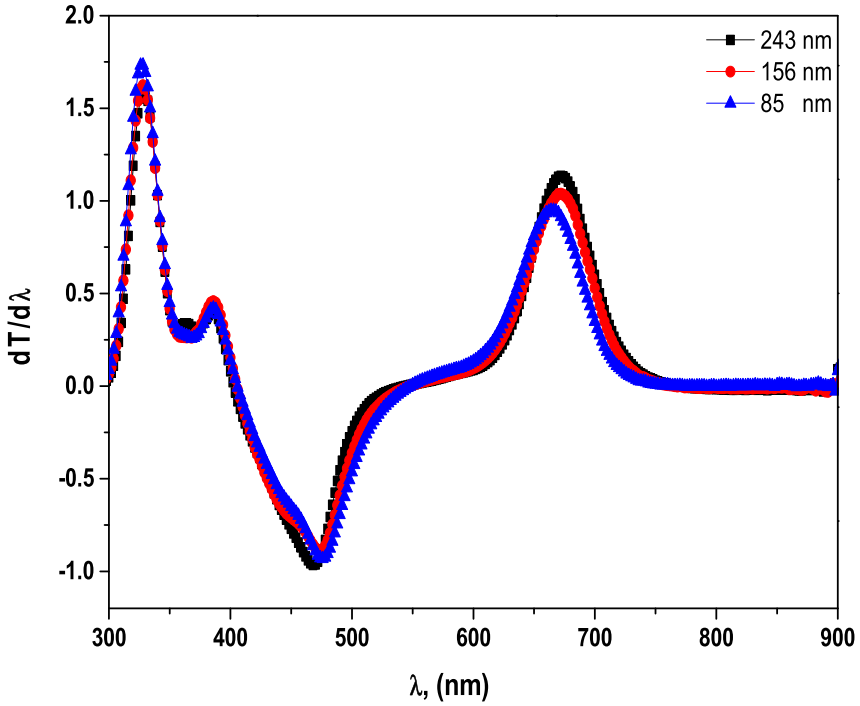

Fig. 4. First derivatives of the transmission spectra for MV-10B thin films of different thicknesses.

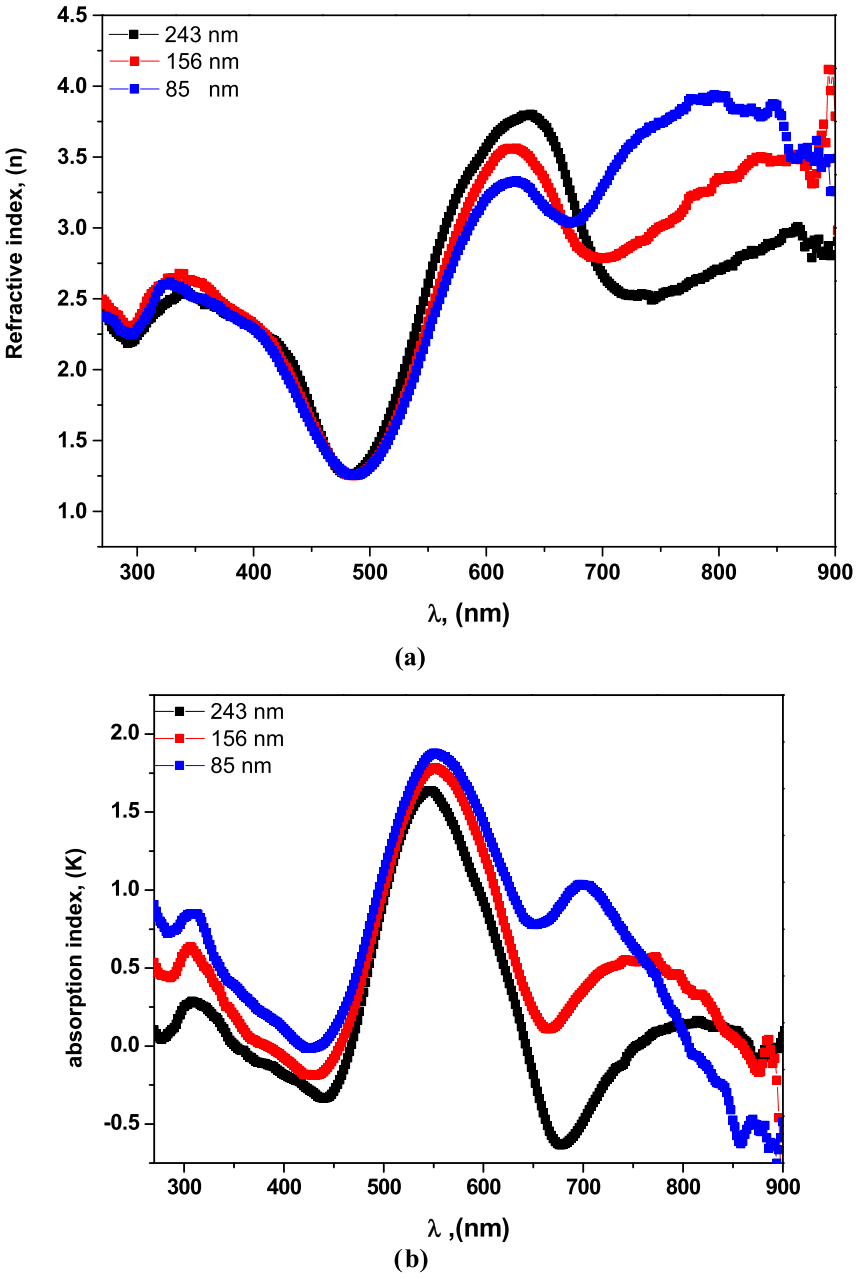

Fig. 5. (a) Refractive index and (b) absorption index calculated using K-K relations.

3. Results and discussions

3.1. X-ray diffraction and atomic force microscopy of MV-10B nanostructured thin films

Fig. 1 displayed the XRD patterns of MV-10B films prepared at diverse rpm. From the figure, the films exhibit a halo in the 2θ range of 20–30°, indicating their amorphous structure [19]. Fig. 2 shows the 3D-AFM image of the MV-10B thin films of thickness 156 nm as a representative example. The image displays vertical growth of needle-like structures eventually resulting in spherically shaped nanoclusters on top of the film. The grain size of these particles was analyzed by Park system XEI software attached to the AFM machine and the mean values of the grain sizes are found to be 23.8 nm with film roughness = 42.98 nm.

3.2. Linear optics of MV-10B nanostructured thin films

3.2.1. Theoretical background of Kramers-Kronig relations

Optical spectroscopy is undoubtedly one of the best and commonly used procedures to gather information regarding the physical characteristics of thin film materials. However, the type of substrate and growth condition strongly influences the optical spectrum and hence the data analysis is typically not so easy. As a result, extraction of refractive index, n, and extinction/absorption coefficient/index, k, is vital to understanding the optical properties of the studied film [20]. A common procedure to assess the complex refractive index ($N' = n + ik$) of films comprises measurement of the normal incidence reflection (R) and transmission (T) data. But, it is not trivial to infer $N'(\omega)$ from the measured R and T and requires solving of complicated rules for R and T in terms of n and k by an iterative procedure involving successive approximations. Besides, this scheme often results in multiple solutions and even ends up in very inaccurate solutions. Denton et al. (1972)

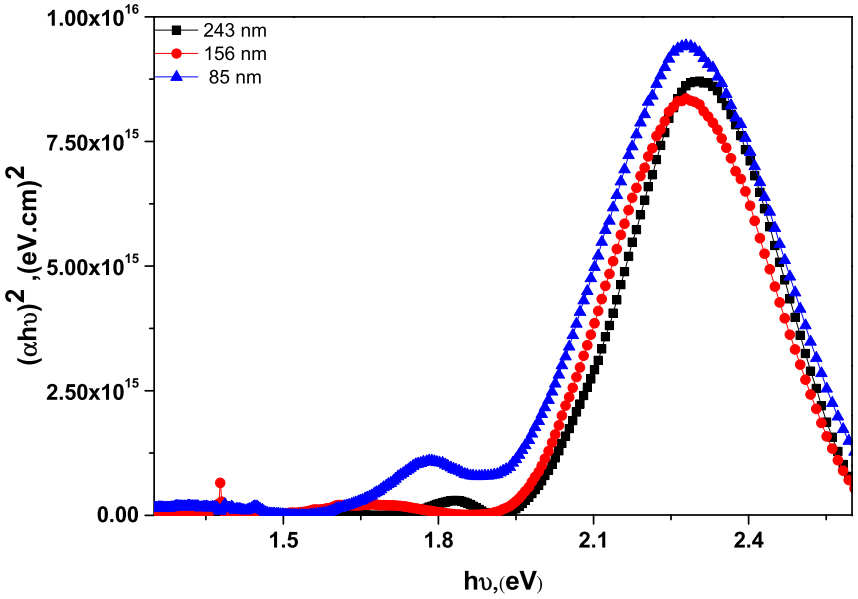

Fig. 6. Tauc's plot for the direct band calculation for MV-10B films.

formulated a new scheme using *(1-R)/T* and *(1 + R)/T* instead of *R* and *T* and ignoring the inappropriate results along with slightly modifying the *R*, *T*, and film thickness until obtaining a plausible solution [21]. A method has been established to calculate *n* and *k* from recorded normal incidence *R* and *T* values, which overcomes the two problems stated above, i.e., without requiring any fine-tuning of the measured data and consideration about the feasibility of the solutions. The method encompasses usage of an iterative procedure to get optical constants using successive approximation results for *T(n,k)* and *R(n,k)* combined with Kramers-Kronig analysis of the transmission data to reach in a viable solution. Kramers-Kronig dispersion relations can be used to estimate the *n* and *k* values from reflectance data even when data is available only for a narrow spectral range. It neither requires any assumptions regarding the out of the experimental range reflectance data nor any extrapolations of the data [22–24]. The Kramers-Kronig method was used to compute the optical constants (*n* and *k*) of the MV-10B thin films from the reflectance data. The *N′* is given by Ref. [25]:

$$N'(\omega) = n(\omega) + ik(\omega), \tag{1}$$

where

$$n(\omega) = \frac{1 - R(\omega)}{1 + R(\omega) - 2\sqrt{R(\omega)}cos\phi(\omega)}, \tag{2}$$

$$k(\omega) = \frac{1 - R(\omega)sin\phi(\omega)}{1 + R(\omega) - 2\sqrt{R(\omega)}cos\phi(\omega)}, \tag{3}$$

and

$$\phi(\omega) = \frac{-\omega}{\pi}\int_0^{\infty} \frac{\ln R(\omega') - ln\ R(\omega)}{\omega'^2 - \omega^2} d\omega', \tag{4}$$

Eq. (4) can be described as:

$$\Phi(\omega_j) = \frac{4\omega_j}{\pi} \times \Delta\,\omega \times \sum_i \frac{\ln(\sqrt{R(\omega)})}{\omega_i^2 - \omega_j^2}, \tag{5}$$

The spectral behavior of *T(λ)*, *Abs(λ)* and *R(λ)* for MV-10B films are presented in Fig. 3(a–c). Two transmission edges are seen in the figure in the range of (341–348 nm) and (392–394 nm). Here, the first one characterizes as the onset of the absorption edge. Also, an opposite edge can be seen in the figure in the wavelength range 445–431 nm, which is an optical absorption edge and effectively creates a valley in the transmission spectra between the absorption edge and 702 nm. The spectra has two prominent regions: (a) the absorption region ($\lambda < 702$ nm) where the sum of *T(λ)* and *R(λ)* is less than unity and (b) the transparent region ($\lambda > 702$ nm) where the film turn into transparent without effective light absorption, $T(\lambda) + R(\lambda) \approx 1$. This is evident from the Fig. 3c as well. It can also be seen from the Fig. 3a–c that the amplitude of transmittance and reflectance increases with the thicknesses in the transparent region while it exhibits an opposite trend in the absorption region. From the figure, the sample exhibit bandpass filter characteristics in IR region i.e. from 700 nm to 900 nm and in a visible range centered around 408 nm. Also, the sample absorbs or attenuates the range of wavelengths in the visible spectrum between 470 and 650 nm creating a good absorption band valley making a CUT-OFF laser filter. Part of the light is absorbed in this region and the rest is reflected allowing only a small percentage to pass through. The measurement of maxima in the first derivative of the transmission data with respect to the incident wavelength, at the lower energy region, gives an easy method to estimate the band gap of the as-prepared thin films [26]. Fig. 4 shows the calculated first derivatives of the transmission spectra against wavelength for MV-10B films deposited at different rpm and the inferred band gap values are 1.848 eV, 1.851 eV and 1.865 eV analogous to the wavelengths 672, 671 and 666 nm, for the corresponding thicknesses 243, 156 and 85, respectively.

Fig. 5(a&b) represent the plots of refractive index and absorption index with respect to the normal incident wavelength, in the range 270–1000 nm. The refractive index was calculated from K-K relations. The figure shows multiple anomalous and normal dispersion regions in the graph within the range of 270–1000 nm and thus exhibits a multi-oscillator model in this range. The anomalous dispersion can be observed in the ranges < 327 nm, 484–630 nm and above 680 nm while normal dispersion behavior is observed in the ranges 327–484 nm and 635–715 nm for the film prepared at 243 nm. Slight shifts are observed for these ranges with the film thickness. The anomalous dispersion is due to the coupling of electrons in MV-10B film to the oscillating electric field aroused due to the to the resonance effect of the incident light and the electron polarization [27].

Three absorption bands can be seen in the *k*-spectrum in UV and visible range with broad peaks centered around 305, 550 and 743 nm, exhibiting slight shifts with thicknesses. From this figure, the values of *k* increase with thicknesses while the *n* values show many crossover points with a thickness in the spectrum indicating that *n* values don't follow a particular scheme in the complete range with the thicknesses. H.M. Zeyada et al. have also noticed the non-dependency of the

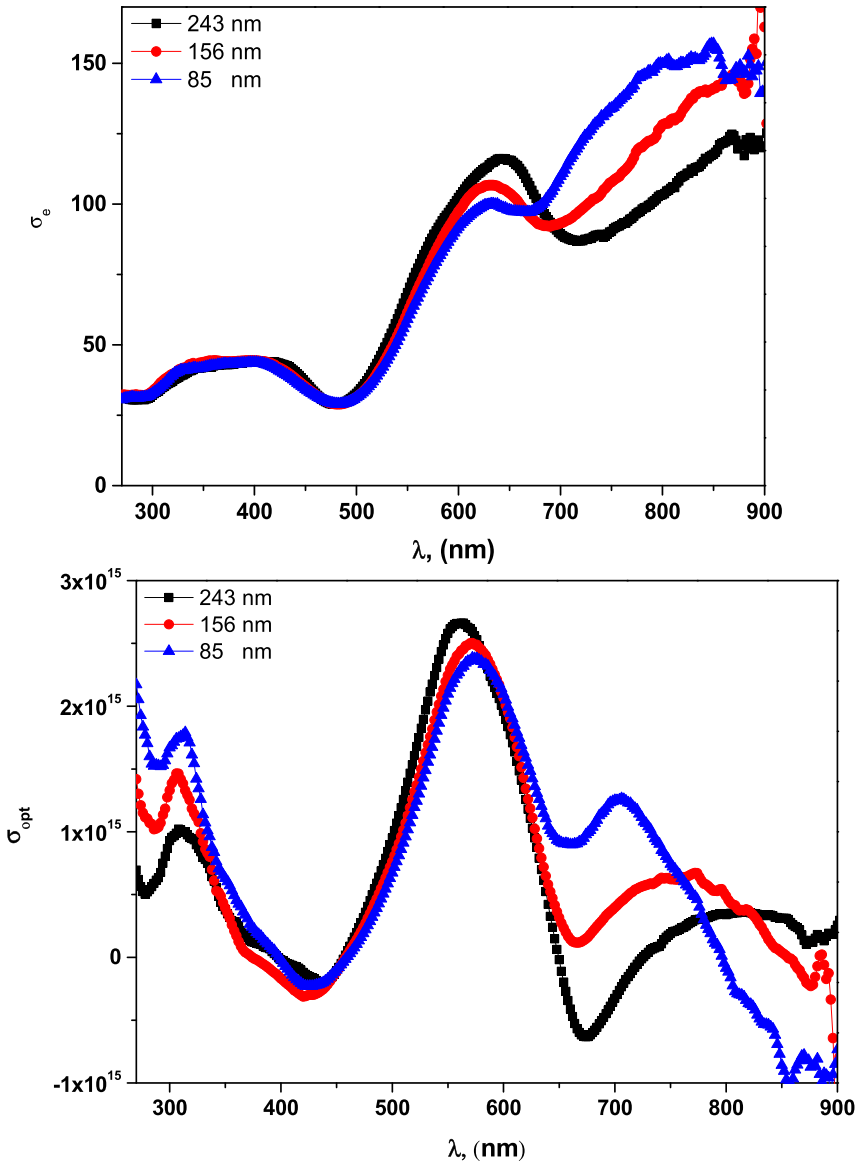

Fig. 7. Electrical and optical conductivity vs. the wavelength for MV-10B films.

refractive index with film thickness, for MV-2B the films prepared by spin coating method [10]. However, in the small range 410–665 nm, *n* value increases with the thicknesses and at 665–850 nm range, it displays the opposite behavior.

Tauc's model is one of the most widely applied techniques to analyze the optical properties of an amorphous material which lets to obtain the band gap energy, E_g, from the coefficient of absorption, α, and energy E. Band gap values of the MV-10B films was calculated by Tauc's model [28,29]

$$\alpha h\nu = A(h\nu - E_g)^n \tag{6}$$

where the value of '*n*' determines the nature of optical transition [30,31]. Herein, the data were best fitted with direct band gap transition corresponding to $n = 1/2$.

The characteristic direct band gap Tauc's plots for the MV-10B films are shown in Fig. 6. Band gap energies, E_g, were estimated from $(\alpha h\nu)^2$ versus $h\nu$ plot and are found to be 1.95 eV, 1.92 eV and 1.85 eV for the films as 243, 156 and 86, respectively. It is evident from the graph that the band gap decrease with increasing the thickness and it might be accredited to pronounced nano-growth of the MV-10B thin films with thicknesses.

Optical conductivity is a convenient tool for analyzing the optical response of a material. This is a generalization of electrical conductivity in the alternating field and is strongly dependent on the electronic states in a material. The electrical and optical conductivity (σ_e and σ_{opt}) can be estimated from the experimental absorption coefficient α, using the relations [32]:

$$\sigma_{opt} = \alpha nc/4\pi, \tag{7}$$

and

$$\sigma_e = 2\lambda\sigma_{opt}/\alpha, \tag{8}$$

here *n* is refractive index and *c* is velocity the of light. Fig. 7(a&b) demonstrates the electrical and optical conductivity with respect to the wavelength for the MV-10B films prepared at different thicknesses. From this Fig. 7a, the general trend of σ_e is to increase with wavelength, which is also obvious from the formula, $\sigma_e = 2\lambda\sigma/\alpha$. The σ_e displays an inverse relationship with the film thickness and could be due to the lowering of film thickness. However, after 700 nm, it reverses the trend and the σ_e increases with decreasing the thickness values. This could be attributed to the comparatively smaller values of absorption coefficient α, with smaller thickness films, where σ_e is inversely proportional to α.

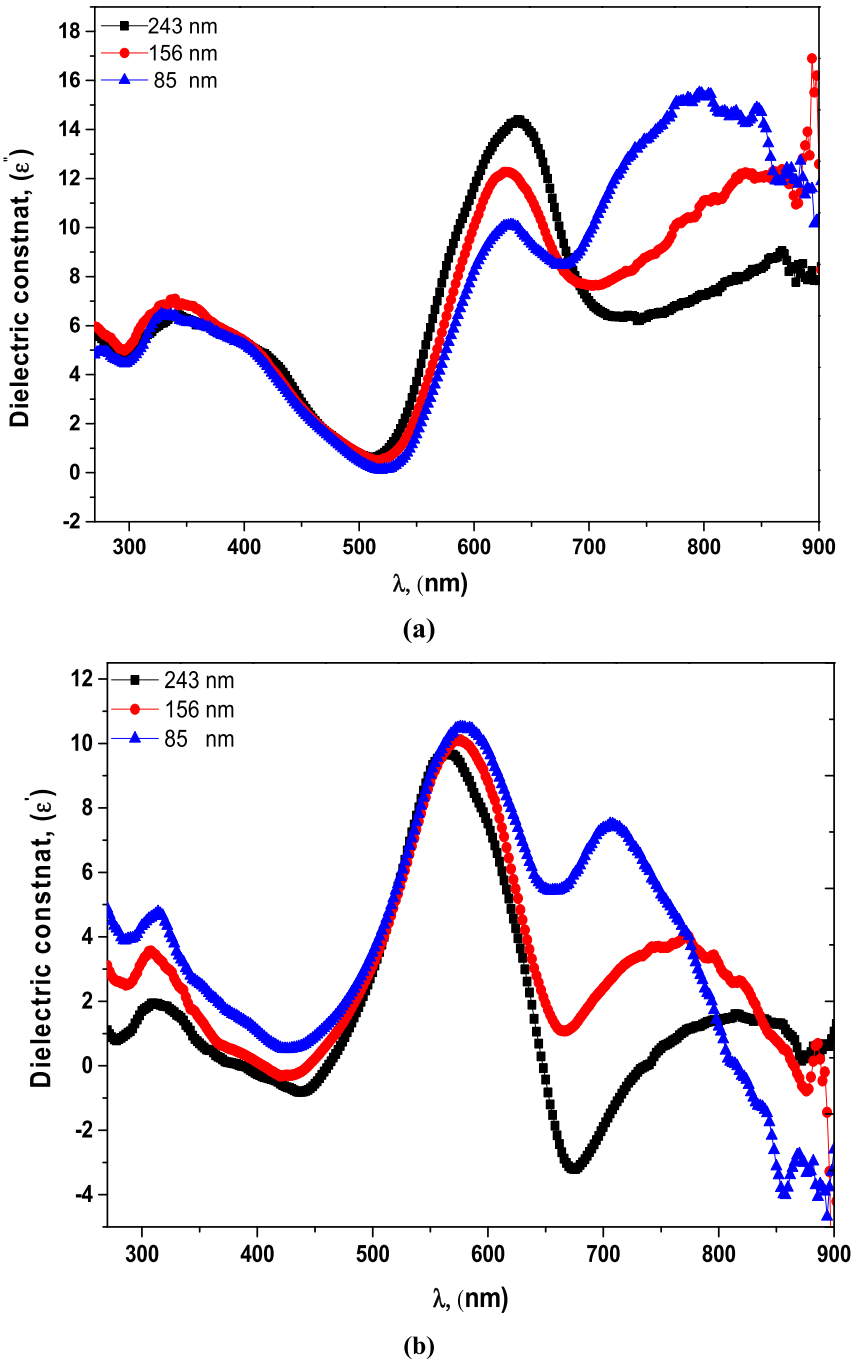

Fig. 8. Spectral behaviors of ε' and ε'' versus λ for MV-10B thin films of different thicknesses.

The optical conductivity outlines the free carriers in the semiconductor [33]. From the Fig. 7b, the optical conductivity decreases with wavelength, when it is moving from the UV-side to the visible side, until 450 nm and then increases sharply giving a wide band between 450 nm and 700 nm. It can be explained as follows: Initially, high photoconductivity was observed in the UV-region as the available free charges absorb incident photon energy and it decreases as the energy of the incident photon decreases. The sharp band in the conductivity spectrum corresponds to the band stop region observed in the transmission and absorption spectra (Fig. 3(a&b)) which is observed as a highly absorbing region for the MV-10B thin films. The valleys in the spectrum indicate that the free charge carriers are trapped.

The optical response of the intervening substance at all frequencies of incident light can be explained by the complex dielectric function, $\tilde{\varepsilon} = \varepsilon' + i\varepsilon''$ [34]. The square of the complex refractive index gives the dielectric function. Thus, the real and imaginary components of the dielectric function can be evaluated using the relations:

$$\tilde{\varepsilon} = \varepsilon' + i\varepsilon'' = [\tilde{N}]^2 = [n + ik]^2, \quad (9)$$

By solving the above equations, the real and imaginary parts of the dielectric functions, ε'& ε'' are related with n and k as [35]:

$$\varepsilon' = n^2 - k^2, \quad (10)$$

$$\varepsilon'' = 2nk, \quad (11)$$

Fig. 8(a&b) represent the plot of real as well as imaginary parts (ε' and ε'') of dielectric constant versus wavelength measured in the UV–Vis regions, for MV-10B thin films prepared with different thicknesses. Absorption peaks for ε' are clear at 1.53, 2.19, and 3.97 eV

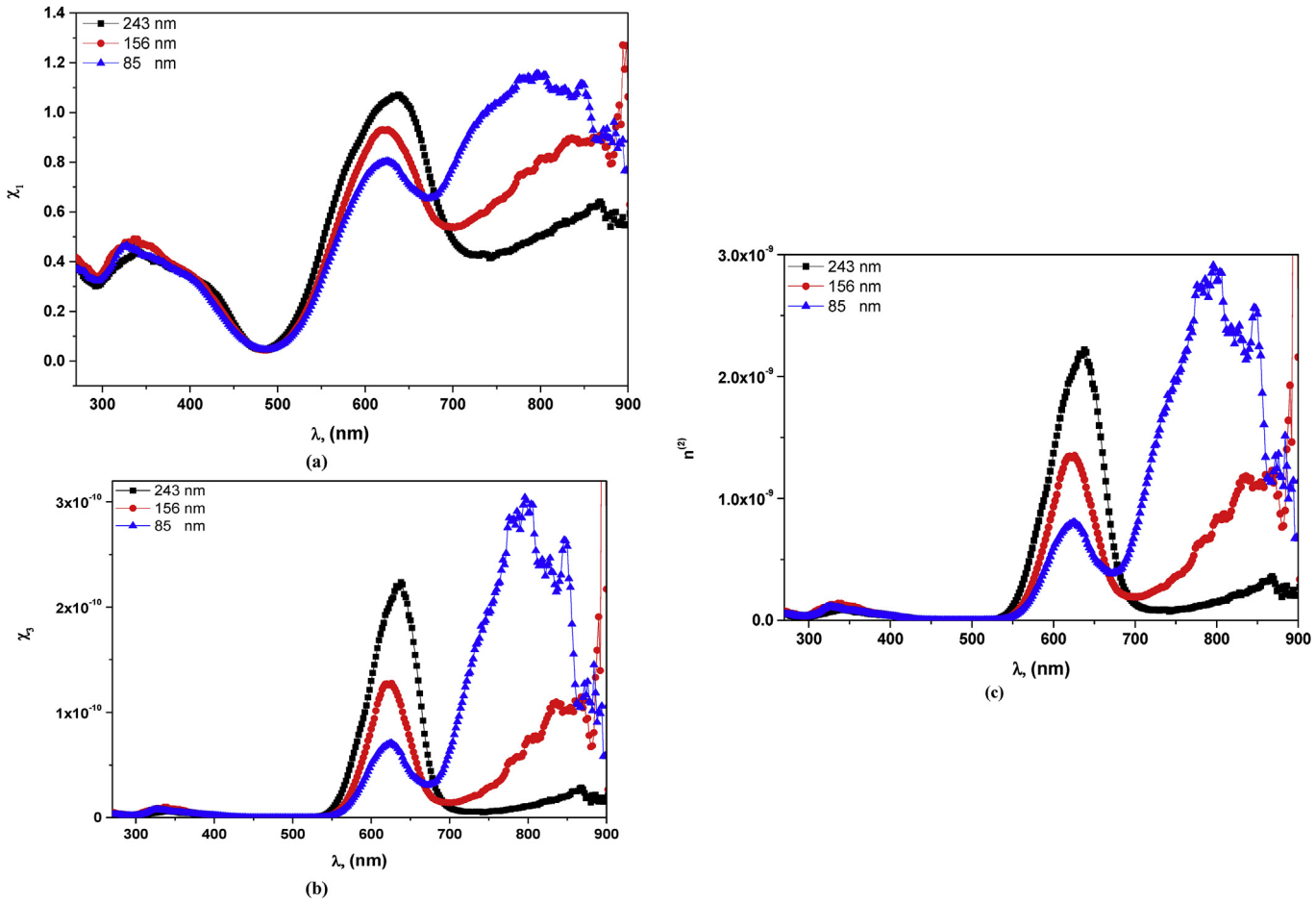

Fig. 9. Spectral behaviors of (a) linear optical susceptibility, $\chi^{(1)}$, (b) nonlinear optical susceptibility $\chi^{(3)}$ and nonlinear refractive index $n^{(2)}$ versus λ for MV-10B thin films of different thicknesses.

Table 1
Optical limiting parameters for the MV-10B thin films of different thicknesses.

The input Intensity of (I_o)	For He-Ne laser at 632.8 nm I_o = 343.1 μW		For green laser at 532 nm I_o = 13.62 mW	
Samples/ Thickness (nm)	Output power (μW)	Normalized power = output power/input power	Output power (mW)	Normalized power = output power/input power
243 nm	26.11	0.076	3.900	0.286
153 nm	96.46	0.281	5.562	0.408
85 nm	120.02	0.350	6.980	0.518

corresponding to 814, 566 and 313 nm for the MV-10B film of thickness 243 nm. With decreasing the film thicknesses, the peak intensities increased. A distinct blue shift of the broad peak centered at 814 nm (for 243 nm) to 706 nm (for 85 nm thickness) was also observed with a reduction in the broadness of the peak. The other peaks displayed redshift of the peak with deca rease in the film thickness. The spectral distribution of ε'' for MV-10B films are shown in Fig. 8b. The graph shows absorption peaks at 867, 639 and 340 nm corresponding to 1.43, 1.94 and 3.65 eV for the film of thickness 243 nm. Blue shift of the broad peak in the lower energy side was also observed with decrease of a film thickness. The intensity of ε' and ε'' is increased with decrease the film thickness in lower energy region and could be ascribed to increase in free carrier density.

3.3. Nonlinear studies of MV-10B in films

Organic, especially dye based thin films possess high nonlinear optical susceptibilities which provide extensive details of the film and hence understanding of how the light rays behave through them is very significant [36–38]. A convincing relation to evaluating the nonlinearity of refractive index and optical polarizability of thin films is given by Ref. [38]:

$$P = \chi^{(1)} E + P_{nl}, \tag{12a}$$

and

$$P_{nl} = \chi^{(1)} E^2 + \chi^{(3)} E^3, \tag{12b}$$

where P is polarizability, $\chi^{(1)}$ is linear susceptibility, whereas the second and third order nonlinear susceptibilities are designated by $\chi^{(2)}$ and $\chi^{(3)}$, respectively [39]. Moreover, the linear refractive index, $n(\lambda)$ could be written as [40]:

$$n(\lambda) = n_0(\lambda) + n_2(E^2), \tag{13}$$

where $(E)^2$ is mean square of electric field [41]. Usually, $n_0(\lambda) \gg n_2(\lambda)$ resulting in $n(\lambda) = n_0(\lambda)$. The $\chi^{(1)}$ is given by the expression [38,39]:

$$\chi^{(1)} = \frac{n^2 - 1}{4\pi}, \tag{14}$$

while the third order nonlinear susceptibility $\chi^{(3)}$ is related to $\chi^{(1)}$ by [ ] [38,39]:

$$\chi^{(3)} = A(\chi^{(1)})^4, \tag{15}$$

and so,

$$\chi^{(3)} = \frac{A}{(4\pi)^4}(n_0^2 - 1)^4, \tag{16}$$

where $A = 1.7 \times 10^{-10}$ esu is a constant [42,43]. The nonlinear refractive index, $n^{(2)}$ has the simple form [44]:

$$n^{(2)} = \frac{12\pi\,\chi^{(3)}}{n_0} \tag{17}$$

Fig. 9(a&b) represent the plots of $\chi^{(1)}$ and $\chi^{(3)}$ with respect to the wavelength for the MV-10B thin films. The graph of $\chi^{(1)}$ strongly resembles that of ε' with a slight shift in the wavelength indicating a strong dependency between the two. The $\chi^{(1)}$ values are found to be in the range of 0.03–1.16. From this figure, both $\chi^{(1)}$ and $\chi^{(2)}$ follow simthe ailar trend in intensity variation against the wavelength for various thicknesses of MV-10B thin films. Fig. 9c portrays the plot of nonlinear refractive index (n_2) with respect to wavelength for the MV-10B thin films. It is a key quantity of the material which offers significant data regarding the light gathering capacity of the film. The graph exactly resembles that of $\chi^{(3)}$ and reveals a very strong reliance of n_2 on $\chi^{(3)}$.

3.4. Optical limiting analysis of MV-10B/FTO thin films

Optical limiters are the systems that attenuate the laser power when passing through it. Due to the large nonlinear behavior of the organic materials, studying the optical limiting properties of organic materials is of significant interest. The optical limiting properties of all deposited MV-10B films are illustrated in Table 1. Tabulated data clearly demonstrates the relationship between the normalized powers for the studied lasers (i.e. He-Ne laser and green lasers) versus MV-10B film thicknesses. The normalized power decreases with thickness and could be owing to higher concentrations of dye available in the path of the laser beam. When the film thickness is higher, more dye molecules are available for the efficient optical interaction in the course of the nonlinear absorption processes to defocus the laser [29]. These results are analogous to the optical limiting properties with varying concentration of dyes both in a liquid medium and thin film samples where people tried varying concentration of dyes on uniform film thickness [45]. These results clearly illustrate that the film thickness and hence the dye concentration available for the interaction with the laser beam has great influence on the optical limiting properties. This result also suggests that MV-10B thin films are promising candidates for many applications in nonlinear media.

4. Conclusion

Nanostructured methyl violet-10B thin films with dissimilar thicknesses were prepared through a spin coating method. It has been found that the prepared MV-10B thin films work like typical direct bandgap semiconductor thin films. XRD studies indicated that the prepared MV-10B thin films were formed in amorphous form. Optical measurements were carried out, and the direct band gap of MV-10B films was estimated. Kramers–Kronig relations were used to getting the real and imaginary parts of the optical constants, n, and k. Non-linear susceptibility and nonlinear refractive index studies were made on linear refractive index dispersion principle. The direct band gap, high transmission, and band stop filter characteristics make the MV-10B thin films a suitable candidate for appropriate optoelectronic applications. The studied materials have the ability to control the laser power (i.e. laser attenuation) even their thickness in nanometer. MV-10B is a promising material in optoelectronic applications.

Acknowledgment

The authors express their appreciation to the Deanship of Scientific Research at King Khalid University for funding this work through research groups program under Grant Number R.G.P.2/9/38.

References

[1] J. Qiu, J. Dawood, S. Zhang, Chin. Sci. Bull. 59 (2014) 2144–2161.
[2] T. Prakash, Elect. Mater. Lett. 8 (2012) 231–243.
[3] M. Gsanger, D. Bialas, L. Huang, M. Stolte, F. Wurthner, Adv. Mater. 28 (2016) 3615–3645.
[4] Nat. Nanotechnol. 4 (2009) 607.
[5] B.J. Rancatore, C.E. Mauldin, S.-H. Tung, C. Wang, A. Hexemer, J. Strzalka, J.M.J. Fréchet, T. Xu, ACS Nano 4 (2010) 2721–2729.
[6] M. Grätzel, J. Photochem. Photobiol. C Photochem. Rev. 4 (2003) 145–153.
[7] M.K. Nazeeruddin, E. Baranoff, M. Grätzel, Sol. Energy 85 (2011) 1172–1178.
[8] M. Freitag, J. Teuscher, Y. Saygili, X. Zhang, F. Giordano, P. Liska, J. Hua, S.M. Zakeeruddin, J.-E. Moser, M. Grätzel, A. Hagfeldt, Nat. Photon. 11 (2017) 372.
[9] E. Singh, K.S. Kim, G.Y. Yeom, H.S. Nalwa, RSC Adv. 7 (2017) 28234–28290.
[10] H.M. Zeyada, A.A. Habashi, M.M. Makhlouf, A.S. Behairy, M.A. Nasher, Microelectron. Eng. 163 (2016) 134–139.
[11] K. Saeed, I. Khan, T. Gul, M. Sadiq, Appl. Water Sci. 7 (2017) 3841–3848.
[12] L.R. Bonetto, F. Ferrarini, C. de Marco, J.S. Crespo, R. Guégan, M. Giovanela, J. Water Process Eng. 6 (2015) 11–20.
[13] M.K. Dahri, M.R.R. Kooh, L.B.L. Lim, ISRN Environ. Chem. 2013 (2013) 8.
[14] K. Tennakone, G.R.R.A. Kumara, A.R. Kumarasinghe, P.M. Sirimanne, J. Photochem. Photobiol. Chem. 96 (1996) 167–169.
[15] A.S. Radwan, M.M. Makhlouf, E. Abdel-Latif, Dyes Pigments 134 (2016) 516–525.
[16] J. Mobley, K.R. Waters, M.S. Hughes, C.S. Hall, J.N. Marsh, G.H. Brandenburger, J.G. Miller, J. Acoust. Soc. Am. 108 (2000) 2091–2106.
[17] J.E. Nestell, R.W. Christy, Appl. Opt. 11 (1972) 643–651.
[18] H. Zahran, I. Yahia, F. Alamri, Phys. B Condens. Matter 513 (2017) 95–102.
[19] M.A. Zeeshan, D. Esque-de Los Ojos, P. Castro-Hartmann, M. Guerrero, J. Nogues, S. Surinach, M.D. Baro, B.J. Nelson, S. Pane, E. Pellicer, J. Sort, Nanoscale 8 (2016) 1344–1351.
[20] R. Nitsche, T. Fritz, Phys. Rev. B 70 (2004) 195432.
[21] R.E. Denton, R.D. Campbell, S.G. Tomlin, J. Phys. D Appl. Phys. 5 (1972) 852.
[22] D.M. Roessler, Br. J. Appl. Phys. 16 (1965) 1119.
[23] 110 (2005), pp. 27-48.
[24] L.L. KIANG, Chin. J. Phys. 14 (1976) 93–100.
[25] S. Scheel, L. Knöll, D.G. Welsch, Phys. Rev. 60 (1999) 4094–4104.
[26] S.K. Suram, P.F. Newhouse, J.M. Gregoire, ACS Comb. Sci. 18 (2016) 673–681.
[27] M.M. Shehata, H. Kamal, H.M. Hasheme, M.M. El-Nahass, K. Abdelhady, Optic Laser. Technol. 106 (2018) 136–144.
[28] J. Tauc, R. Grigorovici, A. Vancu, Phys. Status Solidi 15 (1966) 627–637.
[29] S.M. El-Bashir, I.S. Yahia, M.A. Binhussain, M.S. AlSalhi, Results Phys. 7 (2017) 1238–1244.
[30] M. Shkir, S. Aarya, R. Singh, M. Arora, G. Bhagavannarayana, T. Senguttuvan, Nanosci. Nanotechnol. Lett. 4 (2012) 405–408.
[31] M. Shkir, S. AlFaify, Sci. Rep. 7 (2017) 16091.
[32] H.S. Bolarinwa, M.U. Onuu, A.Y. Fasasi, S.O. Alayande, L.O. Animasahun, I.O. Abdulsalami, O.G. Fadodun, I.A. Egunjobi, J. Taibah Univ. Sci. 11 (2017) 1245–1258.
[33] R.P.S.M. Lobo, 3 - the Optical Conductivity of High-temperature Superconductors, High-temperature Superconductors, Woodhead Publishing, 2011, pp. 103–146.
[34] P.L. Washington, H.C. Ong, J.Y. Dai, R.P.H. Chang, Appl. Phys. Lett. 72 (1998) 3261–3263.
[35] A.B. Khatibani, S.M. Rozati, Bull. Mater. Sci. 38 (2015) 319–326.
[36] H. El Ouazzani, S. Dabos-Seignon, D. Gindre, K. Iliopoulos, M. Todorova, R. Bakalska, P. Penchev, S. Sotirov, T. Kolev, V. Serbezov, A. Arbaoui, M. Bakasse, B. Sahraoui, J. Phys. Chem. C 116 (2012) 7144–7152.
[37] V.V. Shelkovnikov, V.P. Safonov, A.I. Plekhanov, F.A. Zhuravlev, J. Struct. Chem. 34 (1993) 909–922.
[38] M. Shkir, V. Ganesh, S. AlFaify, I.S. Yahia, J. Mater. Sci. Mater. Electron. 28 (2017) 10573–10581.
[39] M. Frumar, J. Jedelský, B. Frumarová, T. Wágner, M. Hrdlička, J. Non-Cryst. Solids 326–327 (2003) 399–404.
[40] M. Shkir, V. Ganesh, S. AlFaify, I. Yahia, H. Zahran, J. Mater. Sci. Mater. Electron. 29 (2018) 6446–6457.
[41] J. Xia, Y. Liu, X. Qiu, Y. Mao, J. He, L. Chen, Mater. Chem. Phys. 136 (2012) 823–830.
[42] H. Ticha, L. Tichy, J. Optoelectron. Adv. Mater. 4 (2002) 381–386.
[43] R. Adair, L.L. Chase, S.A. Payne, Phys. Rev. B 39 (1989) 3337–3350.
[44] V. Ganesh, M. Shkir, S. AlFaify, I.S. Yahia, H.Y. Zahran, A.F.A. El-Rehim, J. Mol. Struct. 1150 (2017) 523–530.
[45] M.I. Mohammed, I.S. Yahia, Opt. Quant. Electron. 50 (2018) 159.